Orbital moment determination in $(Mn_xFe_{1-x})_3O_4$ nanoparticles

V. L. Pool,[1,2,a)] C. Jolley,[3,4] T. Douglas,[2,3] E. A. Arenholz,[5] and Y. U. Idzerda[1,2]
[1]*Department of Physics, Montana State University, Bozeman, Montana 59717, USA*
[2]*Center for Bio-inspired Nanomaterials, Montana State University, Bozeman, Montana 59717, USA*
[3]*Department of Chemistry and Biochemistry, Montana State University, Bozeman, Montana 59717, USA*
[4]*Astrobiology Biogeocatalysis Research Center, Montana State University, Bozeman, Montana 59717, USA*
[5]*Advanced Light Source, Lawrence Berkeley National Labs, Berkeley, California 94720, USA*

Nanoparticles of $(Mn_xFe_{1-x})_3O_4$ with a concentration ranging from $x = 0$ to 1 and a crystallite size of 14–15 nm were measured using X-ray absorption spectroscopy and X-ray magnetic circular dichroism to determine the ratio of the orbital moment to the spin moment for Mn and Fe. At low Mn concentrations, the Mn substitutes into the host Fe_3O_4 spinel structure as Mn^{2+} in the tetrahedral A-site. The net Fe moment, as identified by the X-ray dichrosim intensity, is found to increase at the lowest Mn concentrations then rapidly decrease until no dichroism is observed at 20% Mn. The average Fe orbit/spin moment ratio is determined to initially be negative and small for pure Fe_3O_4 nanoparticles and quickly go to 0 by 5%–10% Mn addition. The average Mn moment is anti-aligned to the Fe moment with an orbit/spin moment ratio of 0.12 which gradually decreases with Mn concentration.

I. INTRODUCTION

The doping of spinel ferrite nanoparticles (γ-Fe_2O_3 and Fe_3O_4) with magnetic and nonmagnetic substitutional transition metals has demonstrated good control of both moment and anisotropy,[1] with magnetic behavior and dopant occupancy sites often quite different from the bulk behavior. One example is for the biomineralization of $(Mn_xFe_{1-x})_3O_4$ nanoparticles inside protein cage structures, where Mn initially substitutes as Mn^{2+} into the octahedral B-site causing the moment to decrease instead of as Mn^{2+} in the tetrahedral A-site,[1] creating an enhanced moment as occurs in the bulk.[2] It is unclear whether these differences are due to the gentle synthesis conditions of biomineralization, the presence of the protein encapsulation, or the reduced dimensionality of nanoparticles. A comparison of dopant occupation sites and anisotropy energies of similar nanoparticles synthesized under different conditions would be useful.

For noninteracting particles, frequency dependent ac-susceptibility measurements are a useful way to determine anisotropy energies.[1,3] A related parameter to the magneto-crystalline anisotropy energy is the elemental orbital magnetic moment as determined from energy integration of the X-ray magnetic circular dichroism spectra (using the XMCD sum-rules).[4–7] Used predominantly for single crystal thin film geometries, this unique method for separating the orbital moment and the spin moment of each element has utility for nanoparticles, especially those found to be interacting.

II. EXPERIMENTAL

Nanoparticles of $(Mn_xFe_{1-x})_3O_4$ were synthesized with $x = 0$ to 1.0 by a chemical route identical to that used for protein encapsulated particles (the synthesis route used in ref #1 but without inclusion of the protein). Solutions of 12.5 mM $(NH_4)_2Fe(SO_4)_2.6H_2O$ and 12.5 mM $MnCl_2$ were prepared using H_2O that had been sparged with N_2 to remove dissolved oxygen and mixed to obtain the desired $[Fe^{2+}]$:$[Mn^{2+}]$ ratio. The 12.5 mM metal mixture and a deaerated 4.17 mM H_2O_2 solution were added at a rate of 40 ml/h to a deaerated solution of 100 mM NaCl maintained at 65°C while the pH was maintained at 8.5 by addition of deaerated 100 mM NaOH using an autotitrator. Samples were centrifuged and triple washed with de-ionized water in order to remove NaCl and unreacted metal ions. Samples used for X-ray absorption spectroscopy (XAS) and X-ray magnetic circular dichroism (XMCD) measurements were stored in an aqueous suspension and subsequently dried onto Formvar-coated TEM grids, while samples to be used for hard X-ray pair distribution function (PDF) analysis were immediately dried to powder using a vacuum lyophilizer.

The XAS and XMCD measurements were conducted at beamline 4.0.2 of the Advanced Light Source of Berkeley National Laboratories simultaneously in transmission yield (using a Ga photodetector) and total electron yield (in the sample current mode). Absorption measurements were made at room temperature with the photon polarization set at 90% and an alternating applied magnetic field of 0.5 T.

III. RESULTS

The Mn L_{23}-edge XAS spectra for a representative sampling of different Mn concentrations are shown in Fig. 1. The spectra have had a linear background removed, been normalized to the integrated peak area ($L_2 + L_3$), and were energy calibrated by comparing the peak position of a simultaneously collected Mn_3O_4 reference powder spectra (set to 640.05 eV). The evolution of the spectra show that as the Mn

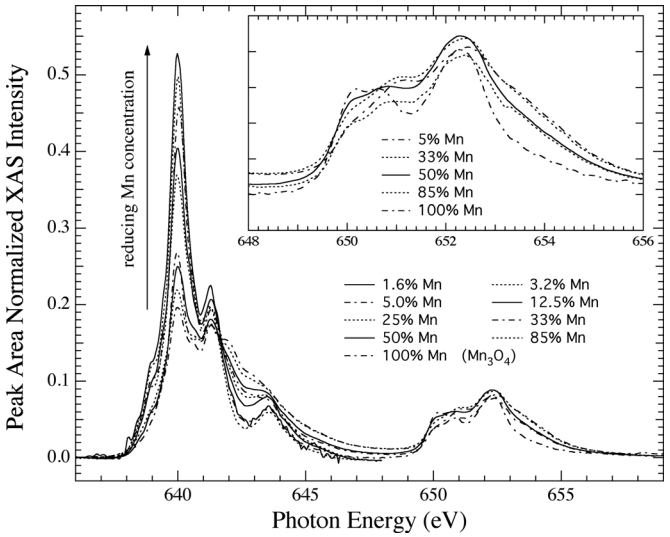

FIG. 1. The evolution of the peak normalized Mn L_{23}-edge XAS spectra as a function of Mn concentration. Inset: Evolution of Mn L_2 peak.

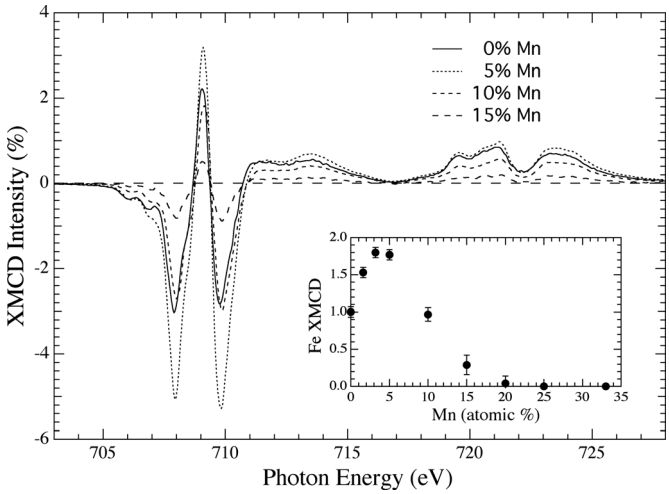

FIG. 2. The evolution of the Fe L_{23}-edge XMCD spectra as a function of Mn concentration. There is no discernable dichroism spectra above 20% Mn Inset: Fe peak-to-peak XMCD intensity as a function of Mn concentration.

concentration is reduced, the Mn L_3 spectral weight shifts dramatically from a broad distribution of higher energy multiplet peaks to the single lower energy peak (the Mn L_2 peak evolves more gradually, see inset of Fig. 1). The final spectrum at 1.6% Mn is nearly identical to the theoretical spectrum for Mn^{2+} in a tetrahedral configuration.[8] The spectra are quite similar for 1.6%–25% Mn concentrations, above which the Mn spectra continue to gradually evolve, but are all similar in shape. This is consistent with the evolution of the crystal structure determined from the hard X-ray scattering PDFs (not shown). From the X-ray scattering PDF, the local Mn structure at high Mn concentrations was identified to be a close match to the hausmannite (Mn_3O_4) structure with a crystalline domain size of 14–15 nm. At low Mn concentrations the PDFs, which are not element specific, closely resemble Fe_3O_4 with a slightly larger crystallite size of 16–18 nm. For all Mn concentrations, the crystalline domain size remains in the 16 ± 2 nm range.

Changes in the Fe XAS spectra have been used to differentiate between the various oxides of Fe.[9,10] Unfortunately, distinguishing between the defective spinel structure of maghemite (γ-Fe_2O_3) and the inverse spinel structure of magnetite (Fe_3O_4) using the subtle variations in the XAS spectra is difficult. A more sensitive method for differentiating between these similar structural phases is the X-ray magnetic circular dichroism (XMCD) spectra of the L_{23} edge.[9,10] Although the total electronic structure, as displayed in the XAS spectra, is rather similar, the spin-resolved electronic structure is better differentiated.

Figure 2 shows the evolution of the Fe XMCD as a function of Mn concentration. The spectra show that the peak-to-peak dichroism signal of Fe first dramatically increases with low Mn addition, then falls rapidly. This behavior, highlighted in the inset of Fig. 2, is well understood if the Mn initially substitutes into the A-site tetrahedral position for the Fe (a conclusion consistent with the subtle evolution of the Fe XAS spectra). In the spinel structure, due to indirect exchange coupling, the magnetic orientation of the Fe in the tetrahedral A-site is opposite the magnetic orientation of Fe in the more numerous octahedral B-site, resulting in an overall reduction in the net Fe moment. Substitution of Mn into the A-site reduces the occupation of Fe in this site, effectively increasing the net Fe moment. This behavior is initially identical to the bulk behavior of $(Mn_xFe_{1-x})_3O_4$, but opposite the behavior recently determined for biomineralization of $(Mn_xFe_{1-x})_3O_4$ into protein cages, where Mn substitutes as Mn^{2+} into the octahedral B-site.[1] Although initially the structural and moment variation between these nonencapsulated nanoparticles and the bulk is similar, above 5% Mn the behavior is found to differ. Whereas the Fe moment in the bulk continues to increase, the moment in the nanoparticles drops rapidly to zero at 25% Mn concentration.

The XMCD spectra have utility beyond determining the relative net moment of an element. High-quality XMCD spectra can also be used to separately determine the elemental spin and orbit components of the moment.[4,5] The orbital moment, μ_{orb}, and spin moment, μ_{spin}, can be obtained from the energy integration of the XMCD, rewritten in a more compact form as[6]

$$\mu_{orb}/\mu_{spin} = \frac{2q}{(9p - 6q)} \quad (1)$$

where μ_{orb} and μ_{spin} are in units of μ_B/atom, q represents the energy integral over the entire XMCD L_{23} edge, and p represents the integral of only the L_3 edge. Here the remaining difficulty is in the separation of the L_3 XMCD signal from the combined edges. When the L_3 XMCD intensity is zero over an extended energy region prior to the L_2 edge, the integrated spectra will have a well-defined plateau, allowing for a straightforward determination of the integral values (p and q).

In Fig. 3 is displayed the energy integral of the Fe L-edge XMCD for Mn concentrations of 0%–15%. The integrals are all well behaved, showing distinct plateau regions, and are quite robust to reasonable variations in the linear background subtraction. An inspection of Eq. (1) shows that if the final value of the integral (q) is zero then the ratio, and therefore the orbital moment, is also zero. We see that for the

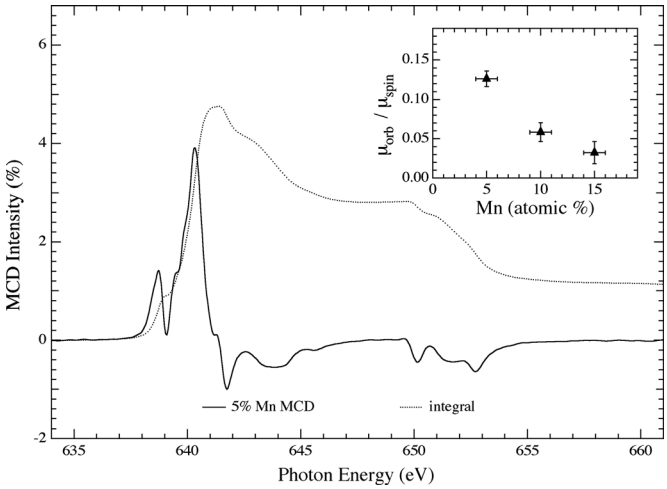

FIG. 3. The integrated Fe L_{23}-edge XMCD spectra for different Mn concentrations. Inset: Mn concentration dependence of the extracted orbital-to-spin magnetic moment ratio for Fe.

defected spinel Fe oxide nanoparticle, the net orbit-to-spin moment ratio for Fe is −0.12. The net orbital moment is small and directed opposite the net spin moment. This can be understood, keeping in mind the multiple sites for the Fe atom. The tetrahedral Fe (A-site) is anti-aligned to the octahedral Fe (B-site). If the orbital moment of the lower symmetry tetrahedral Fe is significantly larger than the orbital moment of the octahedral Fe, then the average orbital moment can be directed opposite to the average spin moment, even though the spin moment and orbit moment of each individual Fe atom are aligned to each other. Significantly, even at the lowest measured Mn concentrations, the extracted net orbital moment for Fe is near zero.

The orbital moment information from the Mn can also be determined. Figure 4 displays the XAS XMCD spectra for the 5% Mn concentration, the energy integrated spectra, and the resulting *p* and *q* integral values. There is remarkable agreement between the Mn MCD spectra and the theoretical

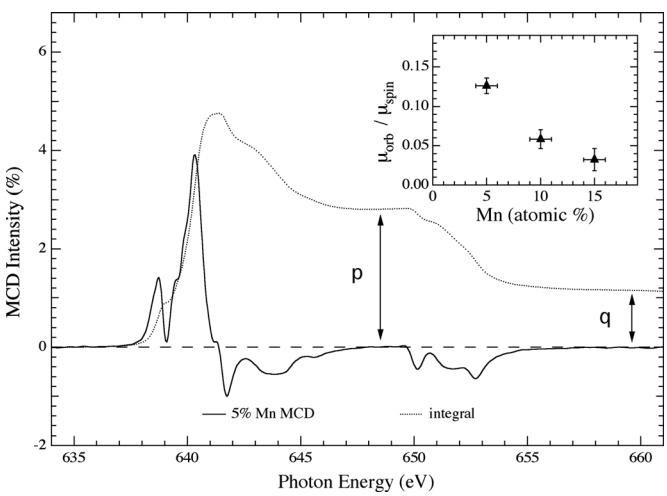

FIG. 4. The Mn L_{23}-edge XMCD spectra for 5% Mn concentration and its energy integral. Inset: Evolution of Mn spin-to-obit moment ratio for Mn.

spectra,[8,11,12] including the separation of the first shoulder of the XAS (first peak of the XMCD) and the subsequent peak, which has not been previously resolved. The evolution of the orbit/spin moment ratio shows a decline in moment to a small value at 15% Mn. Above this concentration, there is a small dichroism spectra, but the energy integrals are not as reliable (not robust to reasonable variations in the linear background subtraction). Below 5%, the XMCD integrals are also not reliable.

IV. CONCLUSIONS

Magnetic nanoparticles of $(Mn_xFe_{1-x})_3O_4$ with a concentration ranging from $x = 0$ to 1 and a crystallite size of 14–15 nm were measured using X-ray absorption spectroscopy and X-ray magnetic circular dichroism spectroscopy to determine the orbital moment to spin moment ratio for Mn and Fe. At low Mn concentrations, the Mn substitutes into the host Fe_3O_4 spinel structure as Mn^{2+} in the tetrahedral A-site, similar to the bulk behavior and not the protein encapsulated nanoparticle behavior, and the Mn XAS and XMCD spectra are in strong agreement with the theoretically predicted spectra. The net Fe moment as identified by the X-ray dichrosim intensity is found to increase at the lowest Mn concentrations then rapidly decrease until no dichroism is observed at 20% Mn in contrast to the bulk behavior.

The elemental Fe orbit/spin moment ratio is determined to initially be small and negative (−0.12) for pure Fe_3O_4 nanoparticles and quickly go to 0 by 5%–10% Mn addition. The net Mn moment is anti-aligned to the Fe moment with a orbit/spin moment ratio of 0.12, which gradually decreases with Mn concentration.

ACKNOWLEDGMENTS

This work is supported by the National Science Foundation (NSF) under grant CBET-0709358 and by the Army Research Office (USARO) under grant W911NF-08-1-0325. The ALS is supported by DOE. under Contract No. DE-AC02-05CH11231.

[1]V. Pool, M. Klem, C. Jolley, E. A. Arenholtz, T. Douglas, M. Young, and Y. U. Idzerda, J. Appl. Phys. **107**, 09B517 (2010).
[2]A. H. Morrish, *The Physical Principles of Magnetism* (IEEE, New York, 2001).
[3]V. Pool, M. Klem, J. Holroyd, T. Harris, T. Douglas, M. Young, and Y. U. Idzerda, J. Appl. Phys. **105**, 07B515 (2009).
[4]B. T. Thole, P. Carra, F. Sette, and G. van der Laan, Phys. Rev. Lett. **68**, 1943 (1992).
[5]P. Carra, B. T. Thole, M. Altarelli, and X. Wang, Phys. Rev. Lett. **70**, 694 (1993).
[6]Y. U. Idzerda, C. T. Chen, H.-J. Lin, H. Tjeng and G. Meigs, Physica B **208/209**, 746 (1995).
[7]C. T. Chen, Y. U. Idzerda, H.-J. Lin, N. V. Tjeng, J. Meigs, E. Chaban, G. H. Ho, E. Pellegrin, and F. Sette, Phys. Rev. Lett. **75**, 152 (1995).
[8]M. P. de Jong, I. Bergenti, V. A. Dediu, M. Fahlman, M. Marsi, and C. Taliani, Phys. Rev. B **71**, 014434 (2005).
[9]H. J. Kim, J. H. Park, and E. Vescovo, Phys. Rev. B **61**, 15284 (2000).
[10]F. Schedin, E. W. Hill, G. van der Laan, and G. Thornton, J. Appl. Phys. **96**, 1165 (2004).
[11]J. S. Kang, G. Kim, H. J. Lee, D. H. Kim, H. S. Kim, J. H. Shim, S. Lee, H. G. Lee, J. Y. Kim, B. H. Kim, and B. I. Min, Phys. Rev. B **77**, 035121 (2008).
[12]S. Brice-Profeta, M.-A. Arrio, E. Tronc, I. Letard, C. Cartier dit Moulin, and P. Sainctavit, Phys. Scr. **T115**, 626 (2005).